Research Report supported by the Reunion Grant for Research Alumni of KIT

Local structure and re-entrance relaxor behavior in $Bi(Mg_{1/2}Ti_{1/2})O_3$-$PbTiO_3$ system

Laijun Liu, Guilin University of Technology, China

Abstract: Synchrotron X-ray diffraction (SXRD) and X-ray pair distribution function (PDF) analyses were used to examine the complex crystal structures of xBi($Mg_{1/2}Ti_{1/2}$)O_3-(1-x)$PbTiO_3$ (xBMT) system. The long-range structure is determined by SXRD while the short-range local structure is characterized from the PDFs. A clear difference can be found between local and average structure. For the sample 50BMT, a strong tetragonal distortion can be found at both local and long-range scale. For the samples 55BMT, 60BMT, 63BMT and 65BMT, PDFs exhibit a local tetragonal distortion although no peak splitting occurs in Bragg diffraction. A box-car fitting analysis of the PDFs gives the local variations at different length scales. The strong distortion scales match the size of nanopolar regions (PNRs) derived from a model analysis of the temperature vs. dielectric response of 65BMT. The results demonstrate that the introduction of BMT into PT disrupts the long-range ferroelectric order of PT, meanwhile, PNRs associated with large local tetragonal/rhombohedral distortions give rise to the re-entrant relaxor behavior.

Introduction

The solid solution xBi($Mg_{1/2}Ti_{1/2}$)O_3-(1-x)$PbTiO_3$ (xBMT-PT) was first reported in 2004. It is considered as an interesting system due to BMT with a structural analogue of anti-ferroelectric $PbZrO_3$. Furthermore, xBMT-PT has also been uniquely shown to possess zero thermal expansion coefficient in the range $0.2 \leq x \leq 0.4$, and highly stable piezoelectric properties at non-ambient temperatures. In terms of the structural phase transition driven by the composition, there is a tetragonal (*P*4*mm*) to monoclinic (*Pm*) phase transition through a mixed phase (*P*4*mm* + *Pm*) region that exists in the range $0.60 \leq x \leq 0.67$, based on the Rietveld refinements of the powder XRD pattern.

The structure description of ferroelectric solid solutions usually is detected by the typical average structural investigation (standard powder diffraction technique). Although there have been rigorous attempts to study particularly the local structural correlations, such as diffuse scattering studies on Pb-based complex systems revealing strong evidence for large deviations from the average structure, there is still lack of an experimentally conceived model at the atomic level to identify and correlate the properties to the different facets of the structure. Hence, there is a pressing need to elucidate mesoscopic-scale atomic correlations in ferroelectric solid solutions to better understand the physics of ferroelectric relaxors.

In this report, we show the composition-driven evolution of the local cation-environment in xBMT-PT as well as their dynamical behavior through a combined analysis of PDFs and temperature dependence of dielectric permittivity for the compounds. Our experimental results provide deeper insights into the local structural evolution of a perovskite-type ferroelectric solid solution and help to establish a comprehensive structure-property relationship for a broad range of systems.

Results and discussion

SXRD patterns of xBMT-PT. The compositions with greater BMT content do not have observable peak splitting in any of the reflections are shown in Fig. 1. The lack of

peak splitting suggests that these compositions have long-range "pseudocubic" symmetry. Rietveld refinements were performed on the SXRD patterns. For 55BMT, an initial space group assignment of *Pm*-3*m* was selected based on the inspection of the peak-splitting. The refinement did not account for anisotropic broadening in several reflections, resulting in a relatively high R_{wp} value. A poor fit with the cubic *Pm*-3*m* space group suggests that the structure has lower-symmetry features, a result that is consistent with the high permittivity (shown later). Of the lower symmetry phases for consideration, *P*4*mm* is logical given the compositional proximity of 50BMT and 55BMT to the *P*4*mm* phase of $PbTiO_3$. However, refinements using a two-phase mixture of space groups *P*4*mm* and *Pm*-3*m* yielded a more reliable solution for all samples compared with single space group, as shown in Fig. 1. The phase fraction of cubic increases with the increase of BMT content except 65BMT. The rhombohedral space group *R*3*m* was chosen which can adequately model the diffraction data. Other common perovskite space groups, *R*3*c* (rhombohedral) or *P*4*bm* (tetragonal), are precluded by the absence of superlattice reflections in the diffraction pattern.

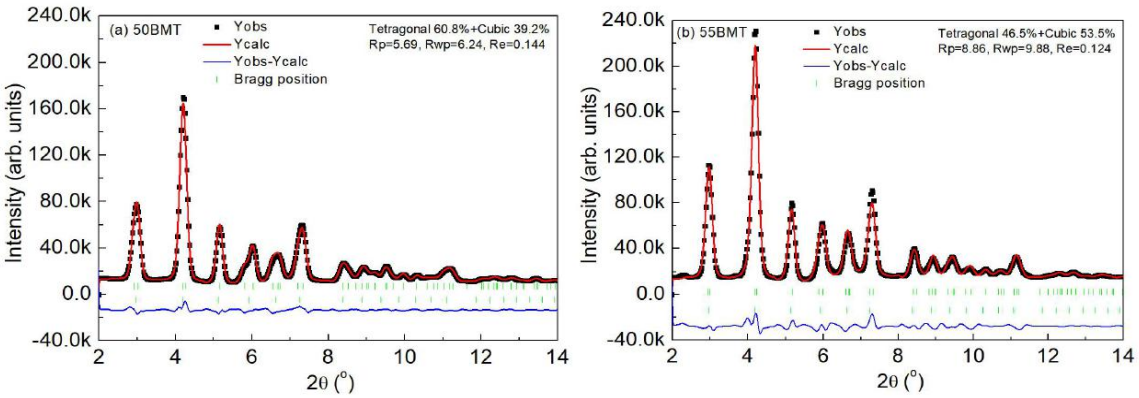

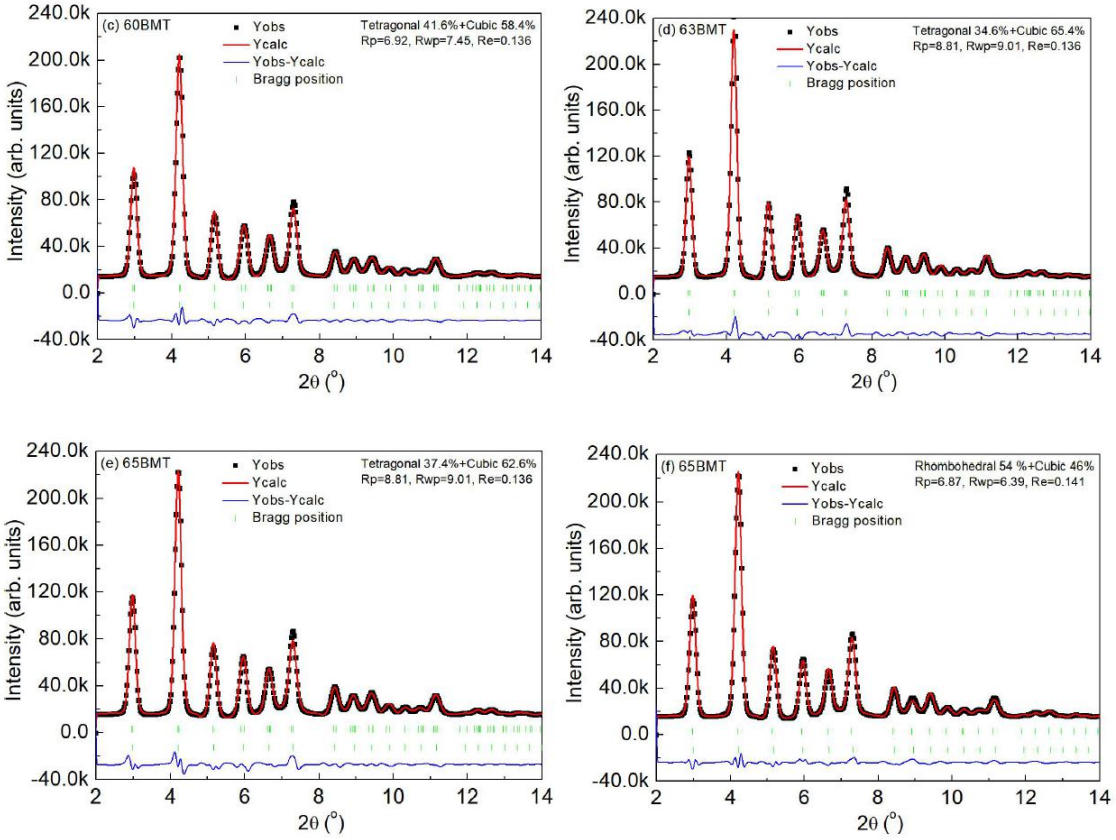

Fig. 1 X-ray Rietveld refinement of *x*BMT-PT using a *Pm*-3*m*+*P*4*mm* structure model for a) 50BMT, b) 55BMT, c) 60 BMT, d) 63BMT and e) 65BMT or a *Pm*-3*m*+*R*3*m* structure model for f) 65 BMT. Data (black symbols) and refined model (red continuous line) are shown, along with the difference pattern (blue) and *hkl* markers (green) below.

The Rietveld refinements of the SXRD patterns characterize the long-range average structure of *x*BMT-PT. However, in some ferroelectric relaxors, the local structure can deviate significantly from the long-range average structure. Pair distribution functions (PDFs) are a useful way of characterizing the local structure and yield the probability of atom-atom pairs as a function of distance *r*. The PDFs of all compositions were initially modeled using a large r-range of 1-60Å. The results of these analyses are shown in Fig. 2. In general, the *c/a* ratio for the structures determined in the large-*r*-range PDF refinement is higher than those determined through Rietveld refinements. Different space groups were trialed in an attempt to identify the best fit

to the PDF data. We first describe the results for 65BMT. The space group *Pm*-3*m* and *R*3*m* did not adequately account for the measured data of 65BMT (R_w~20.2% for *Pm*-3*m* and *17.3%* for *R*3*m*), as shown in Fig. 2(a) and Fig. 2(b). On the other hand, a refinement using the *P*4*mm* space group yielded a lower criterion of fit (R_w~13.2%), which is shown in Fig. 2(c). This result is inconsistent with the space group identification of *R*3*m* determined in the Rietveld refinements using the diffraction data. For other samples, the refinements using the *P*4*mm* space group similarly yielded a lower goodness of fit, and the results are shown in Fig. 2(d)-(g). This result is also consistent with the results of the Rietveld refinement using the diffraction data. The Rietveld refinements using the diffraction data for these compositions indicated a combination of the *P*4*mm* and *Pm*-3*m* phases. Such a phase coexistence was also trialed to model the PDF data, but it was found that adding a *Pm*-3*m* phase only provided a minor improvement to the quality of the fit. Thus, the PDF data of compositions 63BMT, 60BMT, 55BMT and 50BMT are well described using the *P*4*mm* space group. The tetragonal phases of the PDF refinements have slightly higher *c*/*a* ratios than the tetragonal phases of the Rietveld refinements. This initial result suggests that the local structures may be more distorted than the long-range average structure, a conclusion that will be reinforced in subsequent analyses.

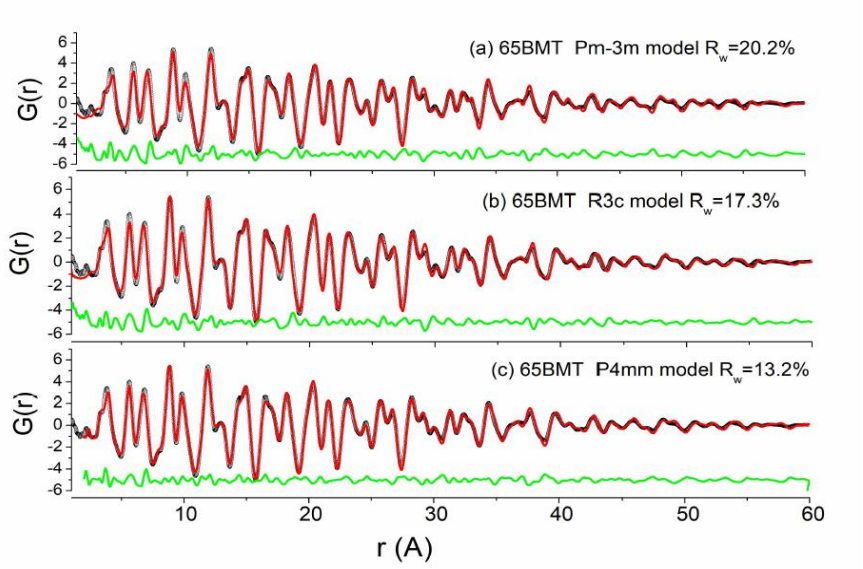

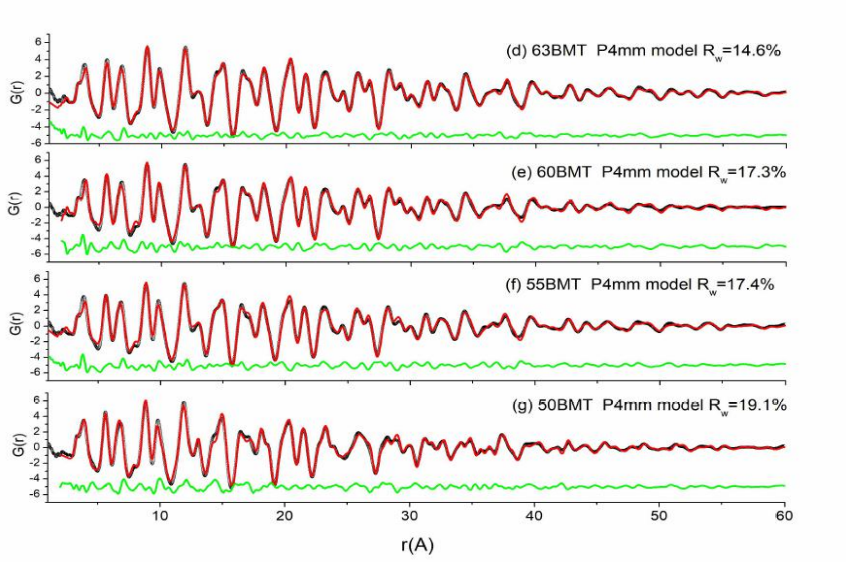

Fig. 2 PDF refinements using the range 1-60Å for 65BMT using a a) *Pm*-3*m*, b) *R*3*m* and c) *P*4*mm* structure model and a *P*4*mm* structure model for d) 63BMT, e) 60BMT, f) 55BMT and g) 50BMT.

The PDFs of *x*BMT-PT are plotted together in Fig. 3. The region from 1~8Å is shown in Fig. 3(a). The first peak around 1.84 Å is associated with the nearest-neighbour Ti-O distances, whereas the broad second peak, appearing at 2.19 Å with increasing *x*, corresponds to the first-neighbour Mg-O distances. The peak around 2.77 Å is related to both A-O and O-O nearest-neighbour distances, which becomes more clear with the decrease of BMT. The shoulder near 3.35Å refers to first-neighbour A-B distances. First neighbour A-A as well as B-B distances are around 3.84 Å. In the low-*r* region, the peaks are at the same positions, indicating that the local structure is constant as a function of composition. As the amount of BMT increases, the PDF peaks at low-*r* decrease in height and increase slightly in width in several pairs, which associates with scattering factors as a function of composition. At high-*r*, it is observed that 50BMT shows different peak heights and positions, exhibiting a clear long-range *P*4*mm* structure. At larger length scales, as shown in Fig. 3(b), the composition 63BMT shows higher peak heights. Since 63BMT is located at the morphotropic phase boundary (MPB), the two phases may have similar local and average atom

distributions, which contribute to higher peak heights.

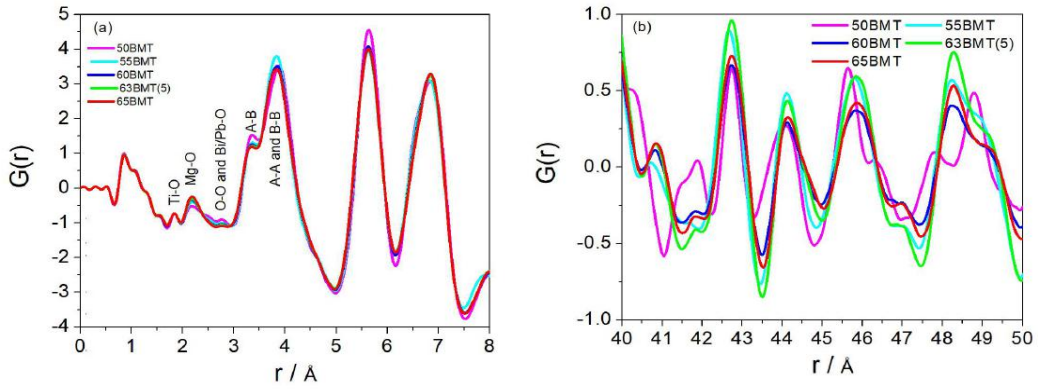

Fig. 3 X-ray PDFs of *x*BMT-PT. a) At low *r*, the peak positions for all compositions are the same, suggesting similar atomic arrangements at the local scale. Additionally, the PDF of the lower-BMT content compositions has higher amplitudes (3.84Å and 5.65Å). b) At higher *r*, the higher peak heights of 63BMT associate with the MPB.

From inspection of the PDFs and the fact that the long-range structures determined from Bragg diffraction and the local structures determined from the PDFs are different, it is observed that *x*BMT-PT exhibits a length-scale dependent structure. In other words, the local structures are different from the long-range, average structures. In order to characterize the length scale dependence of the structure, a box-car fitting technique was performed on the neutron PDFs which allows the structure to be refined as a function of length scale. Fig. 4 shows the variation of the lattice parameters as a function of *r* for each composition from 5 to 60Å. Box-car fitting of the PDFs from 50BMT was undertaken using the single-phase *P*4*mm* space group. The lattice parameters at low *r* show high *c/a* ratios, though for the smallest length probed (1-10Å) there is a slight decrease in tetragonality. It could be attributed to the local-scale rhombohedral-like Ti^{4+}/Mg^{2+} distortion. At higher *r*, the lattice parameters converge to values approximately the same as the long-range, average structure determined from the SXRD Rietveld refinements. In these compositions, the local structure more closely matches the average structure, i.e., it is readily apparent that

both are tetragonal.

For the 55BMT and 60BMT, we reinforce that the most appropriate model for describing the diffraction data (long-range structure) is a two-phase *P*4*mm* and *Pm*-3*m* coexistence, though the most appropriate structure model for describing the local-structure in the PDF data (both box-car fitting and the 1-60Å range fits) is a single *P*4*mm* phase. The PDF box-car fitting reveals that the longer-range structures (20-35Å) of 55BMT and 60BMT are tetragonal, consistent with the *P*4*mm* phase assigned in the Rietveld refinements using diffraction data. Further increasing the fitting range, a very low tetragonal (i.e., small *c/a*) are observed and the cell parameters are close to cubic parameter derived from Rietveld refinements. The local tetragonal distortions "average out" or converge to the long-range lattice parameters as atom-atom distances are calculated across increasing numbers of unit cells.

For the 55BMT and 60BMT with approaching to MPB, in the one or two unit cells range, the cell parameters are close to average structure by the Rietveld refinement with *P*4*mm* space group. Further increasing fitting range, however, a possible rhombohedral distortion occurs near 3-4 unit cells. As a result, the local structure of the compositions near MPB could be a two-phase *P*4*mm* and *R*3*m* coexistence with similar atomic configuration. At the longest distances of 60 Å, there remains a small discrepancy between the pseudocubic lattice parameters determined through the Rietveld refinement and the tetragonal lattice parameters obtained through the refinement of the local structure.

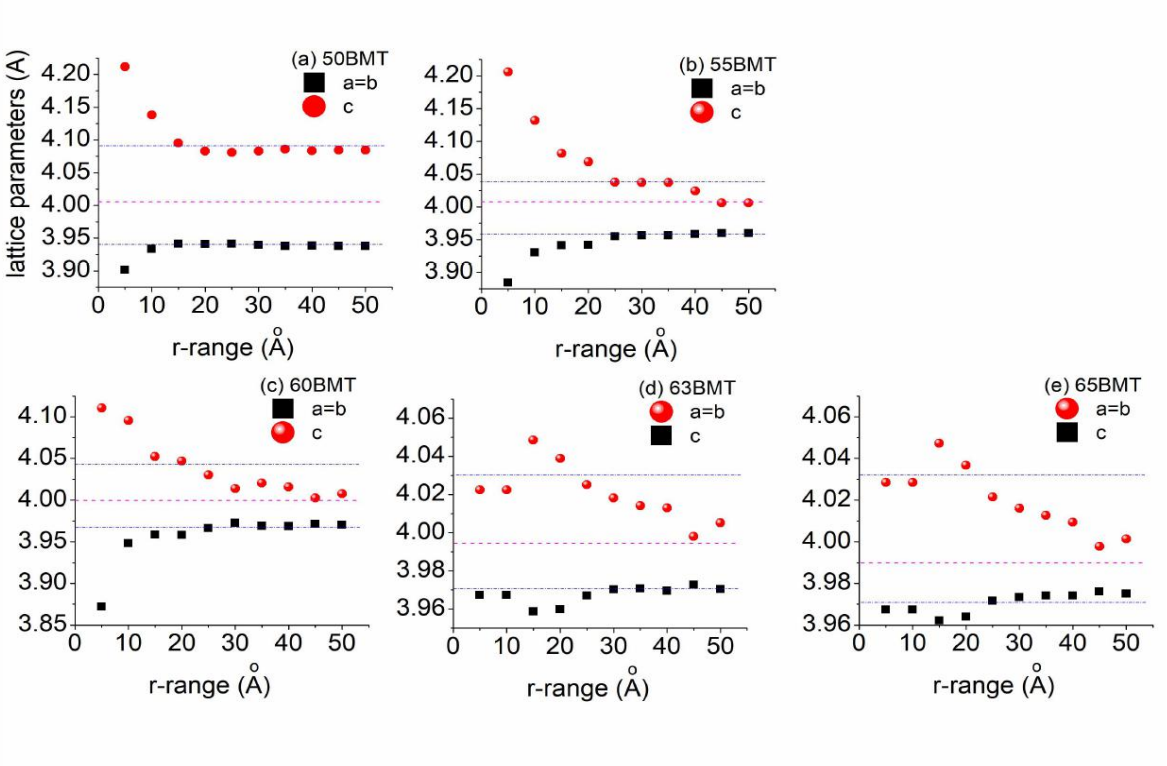

Fig. 4 Results of the box-car analysis of the PDFs for a) 50BMT, b) 55BMT, c) 60BMT, d) 63BMT and e) 65BMT. The analysis resulted in the lattice parameters plotted as red and black symbols. The blue lines indicate the tetragonal lattice parameters obtained from the Rietveld refinements and the dashed pink line represents the lattice parameter for the cubic phase obtained from the Rietveld refinements. Error bars are smaller than the symbols.

These structural findings elucidate the dielectric properties of *x*BMT-PT. Oxides with true cubic symmetry typically have low dielectric constants except extrinsic mechanism. Perovskites with lower symmetry than cubic (either locally or long-range) typically have higher permittivity. Temperature dependence of dielectric permittivity of *x*BMT-PT at different frequencies (100Hz and 1kHz not be shown) are shown in Fig. 5. All the samples include two dielectric anomalies, one occurs near 900K, independent of the concentration of BMT, while the other shows diffuse phase transition (DPT) in 50BMT, furthermore, it becomes DPT with frequency dispersion (relaxor behavior) in 55BMT, 60BMT, 63BMT and 65BMT. Such relaxor behavior originates from a ferroelectric phase rather than a paraelectric phase, named re-entrant

relaxor. SXRD patterns show a cubic symmetry for 55BMT, 60BMT, 63BMT and 65BMT at room temperature, however, a phase separation occurs in these compositions. During cooling, the cubic paraelectric transfers into tetragonal ferroelectric. Upon further cooling, a distorted local rhombohedral (in 63BMT and 65BMT) and a distorted local tetragonal phase (in 55BMT and 60BMT), induced by short-range interaction (polarization) appears. The distorted structure is small in terms of dimension (similar to nanopolar regions) and close to cubic symmetry, which can be described with *Pm*-3*m* space group.

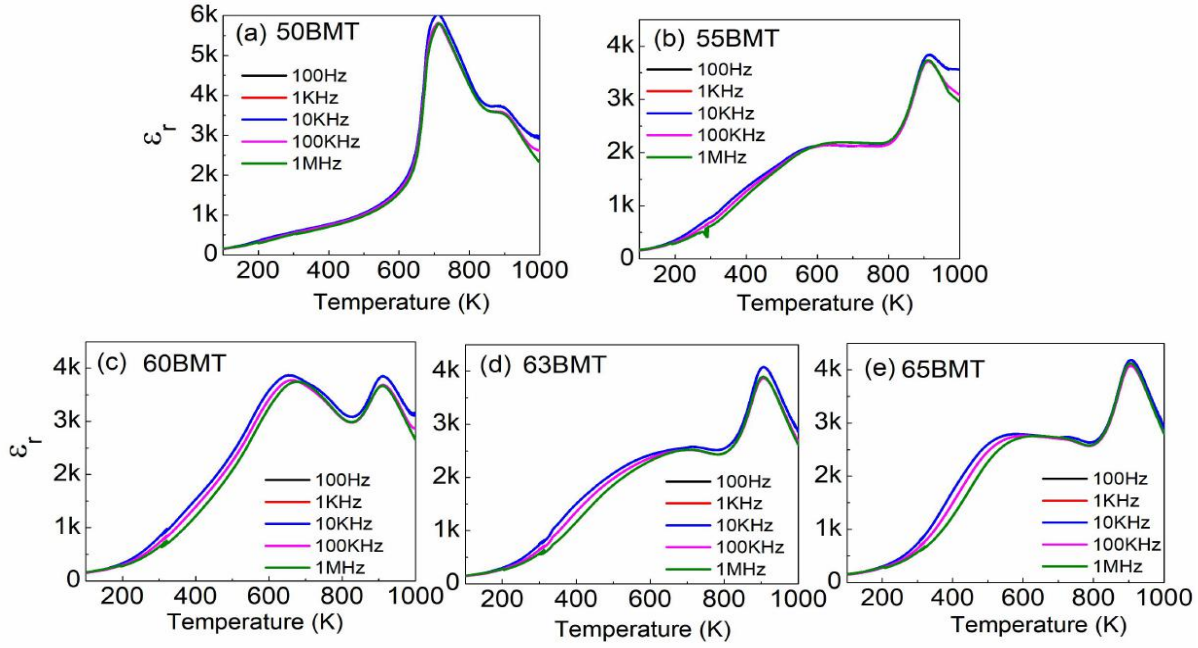

Fig. 5 Permittivity as a function of temperature for (a) 50BMT, (b) 55BMT, (c) 60BMT, (d) 63BMT and (e) 65BMT.

To better describe the relation between dielectric response and local structure, a macroscopic and phenomenological approach [Liu, *et. al*, Phys. Rev. B, 96, 054115 (2017)] was employed to describe the temperature dependence of dielectric permittivity of 65BMT as shown in Fig. 6. A potential well with an average depth (E_b) symbolized for various interactions between dipoles was calculated. The kinetic

energy of dipoles obeys the Maxwell-Boltzmann distribution at corresponding temperature, the number of dipoles with kinetic energy that exceeds the potential well [$N_1(E_b, T)$], and the number of those confined to the potential well [$N_2(E_b, T)$] are given by the following expressions:

$$N_1(E_b,T) = N\sqrt{\frac{4}{\pi}}\sqrt{\frac{E_b}{K_BT}}exp\left(\frac{-E_b}{K_BT}\right) + Nerfc\sqrt{\frac{E_b}{K_BT}} \quad (1)$$

$$N_2(E_b,T) = N - N_1(E_b,T) \quad (2)$$

where N is the total number of dipoles in the system, k_B is the Boltzmann constant (8.617×10^{-5} eV/K), T is the absolute temperature, and *erfc* is the complementary error function. The total susceptibility is described with the following equation:

$$\chi(T,\omega) = \chi_1(T,\omega)P_1(E_b,T) + \chi_2(T,\omega)P_2(E_b,T) \quad (3)$$

where $\chi_1(T,\omega)$ and $\chi_2(T,\omega)$ describe the dielectric responses from the aforementioned two dipole groups, ω is the measurement frequency. $P_1(E_b, T)=N_1(E_b, T)/N$, $P_2(E_b, T)=N_2(E_b, T)/N$ account for the proportion of dipoles in each group. The macroscopic and phenomenological approach was employed to describe the re-entrant dipole glass-like behavior and DPT behavior:

$$\varepsilon(T)_{reentrance} = \frac{\varepsilon_{11}}{1+b_1exp\left(\frac{-\theta_1}{T_1}\right)}P_{11}(E_{b1},T_1) + \varepsilon_{12}P_{12}(E_{b1},T_1) \quad (4)$$

$$\varepsilon(T)_{DPT} = \frac{\varepsilon_{21}}{1+b_2exp\left(\frac{-\theta_2}{T_2}\right)}P_{21}(E_{b2},T_2) + \varepsilon_{22}P_{22}(E_{b2},T_2) \quad (5)$$

$$\varepsilon(T) = \varepsilon(T)_{reentrance} + \varepsilon(T)_{DPT} \quad (6)$$

where ε_{11}, ε_{12}, ε_{21}, ε_{22}, b_1, b_2, θ_1, and θ_2 are constants at a given frequency. One may relate E_b (E_{b1} and/or E_{b2}) to the size of PNRs arising from the local tetragonal/rhombohedral distortion induced by short-range interactions between heterovalent ions. The fitting curves match the experimental data well, suggesting the model can describe well both the re-entrant relaxor and DPT behavior. The E_{b1} of the re-entrant relaxor is ~0.12 eV and the E_{b2} of the DPT behavior is 0.80 eV. According to the Landau-Devonshire formalism of free energy [Haun, *et. al,* Ferroelectrics. 99, 13-86 (1989)], the typical values of $\triangle G$ (energy barrier density for reorientation of a PNR) are in the range of 10^5~10^7 J m^{-3}. Activation energy E_{b1} *or* E_{b2} can be expressed

as $\triangle G^*V$, where V is the volume of a single PNR. The volume of a PNR for re-entrant relaxor and DPF is calculated to be in the range of $(1.92\sim19.23)\times10^{-27}$ m^3 and $(1.28\sim128.17)\times10^{-27}$ m^3, respectively. Correspondingly the size of PNRs ($\sqrt[3]{V}$) for the re-entrant relaxor and the DPF is in the range of 1.24~2.67 nm and 1.07~5.00 nm. Compared with the PDF box-car analysis of 65BMT, the DPF corresponds to a short-range tetragonal distortion present in 1~2 unit cells, while re-entrant relaxor is attributed to a short-range rhombohedral distortion occurring in 4-6 unit cells. Consequently, the relationship between relaxation behavior induced nanopolar regions and local structure is built.

Conclusions

In this report, the long-range and local structures as well as dielectric response of five compositions of 50BMT, 55BMT, 60BMT, 63BMT and 65BMT were characterized. For composition 50BMT, the structure is observed to be locally tetragonal in both the diffraction and PDF data. For compositions of 55BMT, 60BMT, 63BMT and 65BMT, the structure is observed to consist of a two phase average structure, consisting of a pseudocubic phase and a tetragonal phase. The PDF results of compositions confirm that the structure is consistently tetragonal, though diffraction patterns are best modeled using a two-phase coexistence that approximates one of these phases as cubic. The nanoscale regions of polarization present in the compositions provide a mechanism to describe the anomalous dielectric properties such as re-entrant relaxor. Though unobservable by Bragg diffraction, these nanoscale regions of tetragonal/rhombohedral distortions may be the mechanism which is responsible for a large relative permittivity below a DPT. By utilizing SXRD and X-ray PDFs, this work identified local-scale structural features, which update existing structure-property relationships for BMT-PT system and other related compounds.

Acknowledgments

L. Liu acknowledges support from the Reunion Grant for Research Alumni of KIT. I would like to thank Prof. Helmut Ehrenberg and Dr. Manuel Hinterstein's invitation to visit KIT. I also would like to thank Dr. Anna-Lena Hansen and Dr. Michael Knapp and Dr. Frederick Peter Marlton for kind help and the useful discussions. This work has benefited from the use of the beamlines P02.1 at DESY (Synchrotron, Hamburg, Germany) and NOMAD at ORNL (Spallation Neutron Source, Oak Ridge, USA).

****

Neutron diffraction and Neutron PDF results have not finished the fitting.